International Journal of Modern Manufacturing Technologies
ISSN 2067–3604, Vol. XIV, No. 2 / 2022
https://doi.org/ 10.54684/ijmmt.2022.14.2.319

HOT DUCTILITY BEHAVIOR OF Fe-0.05C-24Mn-3.5Si-1.6Al STEEL WITH Nb AND Ti MICROADDITIONS

Gabriela Fojt-Dymara[1], Marek Opiela[2]

[1]Silesian University of Technology, Faculty of Mechanical Engineering, Department of Engineering Processes Automation and Integrated Manufacturing Systems, Konarskiego 18a, 44-100 Gliwice, Poland
[2]Silesian University of Technology, Faculty of Mechanical Engineering, Department of Engineering Materials and Biomaterials, Konarskiego 18a, 44-100 Gliwice, Poland

Corresponding author: Gabriela Fojt-Dymara, gabriela.fojt-dymara@polsl.pl

Abstract: Hot ductility tests were carried out on Fe-0.05C-24Mn-3.5Si-1.6Al high-manganese austenitic steel with Nb and Ti microadditions at a concentration of 0.029% and 0.075%, respectively. Hot tensile tests were performed using Gleeble 3800 thermomechanical simulator on specimens with a diameter of 6 mm and 116.5 mm in length. Deformation was carried out in a temperature range from 1050 °C to 1200 °C with a strain rate of $2.5 \cdot 10^{-3}$ s^{-1} and $5.0 \cdot 10^{-3}$ s^{-1}. Hot ductility was determined on the basis on evaluation of reduction in area (RA). Higher values of stress on the work-hardening curves were observed during tension carried out at higher strain rate. An analysis of the form and course of curves obtained in the tensile test allows to state that, in the studied range of hot plastic deformation parameters, the decrease of strain hardening is caused by the process of dynamic recrystallization (DRX). The reduction in area in a temperature range from 1050 °C to 1200 °C decreases from 90% to approx. 58% for the strain rate of $2.5 \cdot 10^{-3}$ s^{-1} and from 82% to 48% – for the strain rate of $5.0 \cdot 10^{-3}$ s^{-1}.
Key words: high-manganese steel, hot ductility, reduction of area, fracture behavior.

1. INTRODUCTION

Automotive industry belongs to one of the branches of global market which creates continuous demands of constructional materials with higher strength, maintaining required formability, especially drawing, and corrosion resistance. The relation of strength and density of the material, deciding about vehicle's mass and therefore fuel consumption and ecological damages caused by emitted exhaust gas, is also of great importance. Alloys based on Al and Mg as well as polymer composite materials arouse interest because of their low density. Although these materials are increasingly applied in the automotive industry, yet about 60% of car mass consists of constructional parts formed from steel sheets with improved strength, maintaining good plastic properties and formability [1-3].

The positive effect of retained austenite in car body steels has led to increase in the manganese content, which strongly stabilizes the γ phase.

This requires different approach in designing of chemical composition than those used for multiphase steels with ferrite matrix. Extraordinarily advantageous balance between strength and ductility can be obtained in high-manganese steels with homogeneous austenitic microstructure [4-7]. These steels usually consist of 15% to 30% wt% Mn, from 0.02% to 0.08% wt% C and around 3% Al and 3% wt% Si, which are added, among others, to decrease density, which for this group of steels is equal about 7.3 g/cm^3 [8-10]. Beneficial set of mechanical properties that can be obtained for these steels, i.e. ultimate tensile strength (UTS) = 600÷900 MPa, yield strength ($YS_{0.2}$) = 250÷450 MPa and while uniform elongation (UEl) = 35÷80%, strongly depends on chemical composition (stacking fault energy), and in particular on the concentration of Mn, which determines the main strengthening mechanism occurs during technological forming. In addition to the above-mentioned properties, these steels are characterized by particularly high ability to absorb significant amount of energy under high strain rate conditions [11]. The reason for the high work hardening rate and high plasticity in these steels is a gradual course of strain induced martensitic transformation (TRIP effect) [12-15] and/or mechanical twinning (TWIP effect) [16-19].

The issue with wider use of these steels is related to the susceptibility to segregation and difficulties occurring during casting and hot working [20-22]. For instance, during straightening operations in continuous casting of steel [23-25], the ingot surface is subjected to the cyclic impact of guide rolls and plastic strain. Segregation of elements, phase transformations and precipitation processes take place during cooling of steel. At this stage of production,

the surface of steel ingot with low plastic properties is exposed to cracking. Hence, the knowledge of high temperature plasticity allows to optimize the manufacturing process, minimizing the possibility of ingots cracking.
The purpose of the work is to investigate the impact of temperature and strain rate on the course of work-hardening curves and ductility of Fe-0.05C-24Mn-3.5Si-1.6Al high-manganese austenitic steel with Nb and Ti microadditions.

2. MATERIAL AND METHODS

The research was carried out on newly-developed high-Mn austenitic steel with Nb and Ti microadditions. The chemical composition of investigated steel is presented in Table 1.

Table 1. Chemical composition of investigated steel [14]

Elements contents, wt %					
C	**Mn**	**Si**	**Al**	**Nb**	**Ti**
0.054	24.4	3.5	1.6	0.029	0.075

Investigated steel was produced in carefully performed metallurgical process It contains a limited concentration of impurities (0.004% P, 0.016% S) and gases (0.0039% N and 0.0006% O) as well as a negligible amount of non-metallic inclusions, properly modified with Ce and La, in a concentration of 0.058% and 0.020%, respectively.
Introducing Nb and Ti microadditions was to form carbides, nitrides and carbonitrides during hot-working. Presence of these phases allows to obtain fine-grained microstructure of primary austenite. Kang et al. [26] revealed that formation of AlN particles, impeding essentially the course of dynamic recrystallization in C-Mn-Si-Al-Nb type steels with high concentration of Al, can be the cause of decreased hot formability of continuous castings, deformed initially after exiting the catalyst.
Initial processing of ingots was carried out by free forging method on Kawazoe hydraulic press, which resulted in obtaining 20 mm x 200 mm flat bars. Then, flat bars were rolled in a temperature range from 1100°C to 900°C into 6.5 mm thick sheet. The samples were taken from a sheet made according to the scheme shown in Figure 1.
High-temperature tensile tests were carried out on the Gleeble 3800 thermomechanical simulator. Securing nuts were screwed onto screwed ends of the samples, which were successively placed in copper holders. Due to their high thermal conductivity, samples were intensively cooled. Thermocouples, controlling testing temperature with the accuracy of ± 1°C, were welded to the samples. Tests were done in vacuum. The Gleeble 3800 thermomechanical simulator chamber during the tensile test is shown in Fig. 3.

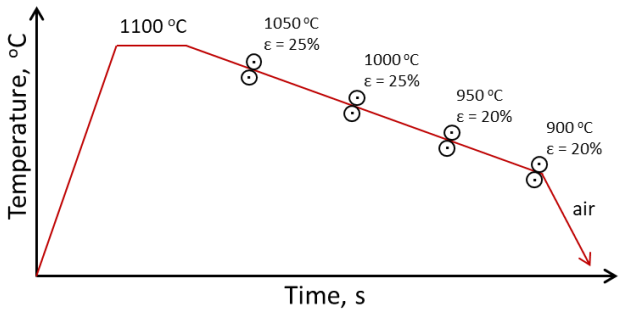

Fig. 1. Scheme of sheet metal rolling

Samples with the shape and dimensions shown in Fig. 2 were taken from the sheets for high-temperature tensile test.

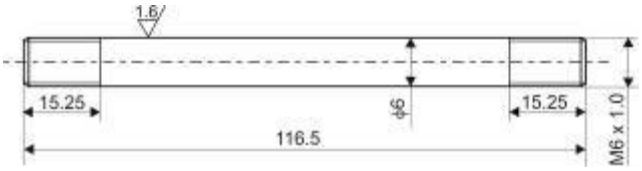

Fig. 2. Shape and dimensions of the sample used in high-temperature tensile test

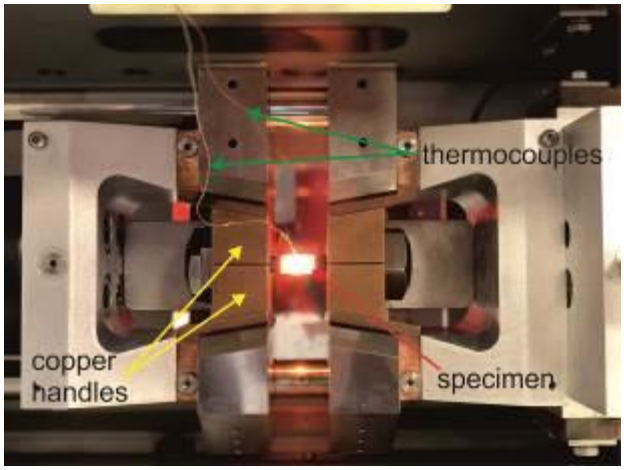

Fig. 3. Gleeble 3800 simulator chamber during high-temperature tensile test

Specimens were resistance heated at the rate of 20 °C/s to the austenitizing temperature 1200 °C, held at this temperature for 120 s, and then cooled to the preset plastic strain temperature of 1050 °C, 1100 °C and 1150 °C (Fig. 4). One of the samples was deformed at the austenitizing temperature, i.e. 1200 °C, using the same holding time as in case of samples deformed at lower temperatures.
Specimens were subjected to tension until fracture at a constant strain rate of $2.5 \cdot 10^{-3}$ s^{-1} and $5 \cdot 10^{-3}$ s^{-1}. After deformation, specimens were cooled to ambient temperature at the rate of 30 °C/s. Three tests were performed for each deformation parameter.

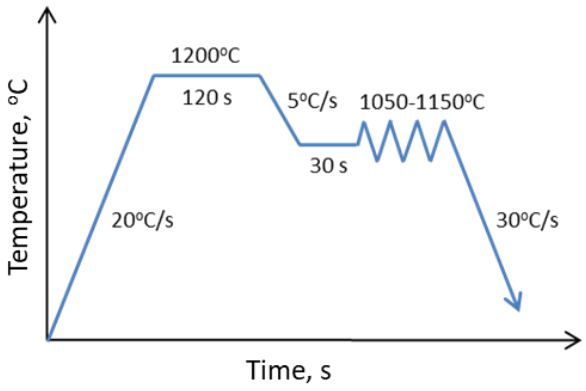

Fig. 4. Scheme of high-temperature tensile test

Hot ductility of tested steel was verified by determining the reduction in area (RA), using the equation (1).

$$RA = (S_0 - S_1)/S_0 \times 100\% \quad (1)$$

where: S_0 and S_1 are original cross section area, and fracture cross section area, respectively.

Preparation of specimens for metallographic tests included standard grinding and mechanical polishing procedures. After that, metallographic specimens were etched in Nital. Metallographic observations were carried out in LEICA MEF 4A light microscope in the magnification range of 100÷500x. Examination of fracture surface after hot tensile tests was done in ZEISS SUPRA 35 high resolution scanning electron microscope, working at accelerating voltage of 25 kV. Observations were performed in a range of magnifications 100÷15000x. Identification of chemical composition of secondary phases precipitations and non-metallic inclusions, revealed at fractures, was carried out using the EDAX TRIDENT XM4 EDS energy dispersive X-ray spectrometer.

3. RESULTS AND DISCUSSION

Examination of the hot plastic deformation process of Fe-0.05C-24Mn-3.5Si-1.6Al steel with Nb and Ti microadditions, performed in a temperature range from 1050 °C to 1200 °C at a strain rate of $2.5 \cdot 10^{-3}$ s^{-1} and $5 \cdot 10^{-3}$ s^{-1}, allowed to determine the influence of tensile parameters at constant austenitizing temperature on the course of work-hardening curves determined in the stress σ – strain ε system.

The form of σ-ε curves of the examined steel, subjected to tension at constant strain rate of $2.5 \cdot 10^{-3}$ s^{-1}, is shown in Fig. 5. Data presented in this figure shows that plastic strain begins at the stress even to the temperature yield point, which decreases along with increase of testing temperature.

An increase of yield stress can be observed on work-hardening curves in a range of strain hardening ε < 0.05, as a result of increasing density of dislocations generated in this process.. Subsequently, at strain increased from ε = 0.05 to ε_m, slight increase of stress takes place up to reaching maximum value of yield stress. This indicates, that thermally activated processes causing partial decay of emitted dislocations, occur along with formation of new dislocations during the plastic strain. After exceeding the value of deformation ε_m, which decreases with increasing test temperature, work-hardening curves show gentle decrease in yield stress.

For the studied temperature range, the stress-strain curves at a rate of $5 \cdot 10^{-3}$ s^{-1} (Fig. 6) show higher values of the σ_m maximum yield stress when compared to the stress - strain curves obtained at a rate of $2.5 \cdot 10^{-3}$ s^{-1}. Along with reduction of temperature and decreasing strain rate, the ε_m deformation value, corresponding to the maximum yield stress, moves towards larger deformations. For the strain rate of $2.5 \cdot 10^{-3}$ s^{-1}, a decrease of plastic strain temperature from 1200 °C to 1050 °C causes an increase in the maximum yield stresses from 16 MPa to 43 MPa and the ε_m deformation from 6 % to 12 %. The decrease of strain temperature in the same temperature range during tension at the rate of $5 \cdot 10^{-3}$ s^{-1} affects an increase of σ_m, from 21 MPa to 58 MPa.

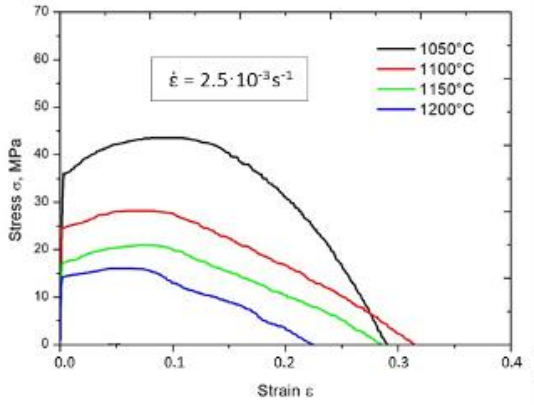

Fig. 5. Influence of plastic deformation temperature on a shape of σ-ε for the high-Mn steel (strain rate $2.5 \cdot 10^{-3}$ s^{-1})

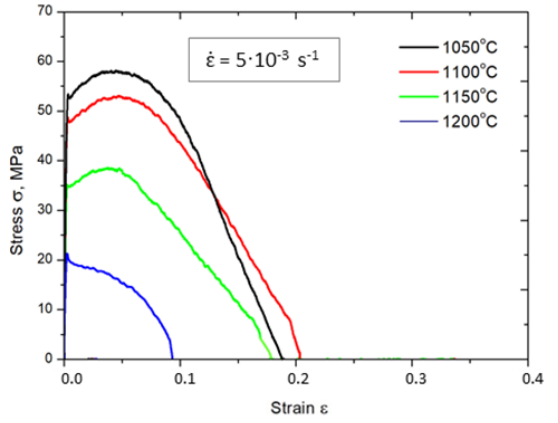

Fig. 6. Influence of plastic deformation temperature on a shape of σ-ε for the high-Mn steel (strain rate $5 \cdot 10^{-3}$ s^{-1})

Hot ductility of the investigated high-manganese steel was determined on the basis of assessment of the reduction in area parameter. An influence of plastic strain temperature and strain rate on the changes of reduction in area is shown in Fig. 7. Figure 7 shows that slightly higher values of the reduction in area for the entire range of applied temperature are noted for specimens deformed at a lower rate.

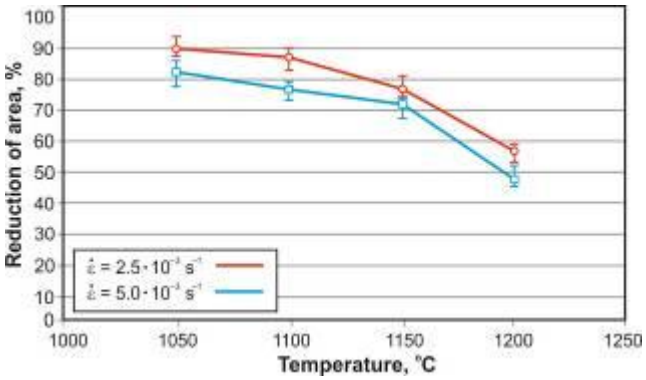

Fig. 7. An influence of plastic deformation temperature and strain rate on the changes of reduction of area

The reduction in area of the samples subjected to tension at this strain rate decreases from 90% at the temperature of 1050 °C and to 58% at the temperature of 1200 °C. The reduction in area of specimens subjected to tension at twice higher rate in the mentioned temperature range is reduced from 82% to 48%.

Macromorphology of samples after hot tensile test is shown in Fig. 8. Macromorphology of samples after performed tensile test fully corresponds to the course of the curves in Fig. 7.

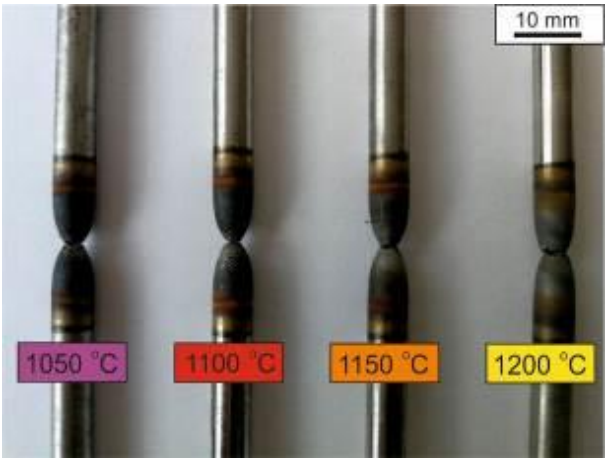

Fig. 8. View of the specimens after the hot tensile test (strain rate $5 \cdot 10^{-3}\ s^{-1}$)

The results of hot ductility tests are similar to the results obtained by Wang and Zhao [27] for steel subjected to hot tensile test in a similar temperature range. According to the data obtained in this study, the reduction in area of samples in a temperature range from 1050 °C to 1200 °C decreased from 87% to 56%. Hot ductility tests of high-manganese Twinning Induced Plasticity (TWIP) type steel were also the subject of research, with the results summarized in the work by Qaban [28]. Steel specimens, containing 0.6% C, 18% Mn, 0.1% Si, 1.5% Al, 0.035% Ti and 0.032% Nb, after austenitizing at the temperature of 1250 °C, were subjected to tension in a temperature range from 700 °C to 1100 °C. Obtained results showed, that in a temperature range from 800 °C to 1000 °C, examined steel is characterized by good hot ductility. The reduction in area of samples tested in this temperature range was over 50%. Increasing the tension temperature to 1100°C resulted in a significant decrease in ductility (RA < 35%). Results of hot ductility tests of steels with chemical composition similar to the analyzed steel were presented in [29-31]. Fractures of examined steel specimens, subjected to tension in a temperature range from 1050 °C to 1200 °C, are presented in Fig. 9. In a strain temperature range from 1050 °C to 1150 °C, studied high-manganese steel, demonstrates ductile fracture with the presence of large number of pits and voids of various sizes and depths (Fig. 10a, b), regardless of the applied strain rate. In mentioned temperature range, investigated steel shows high ductility (RA from 90% at a temperature of 1050 °C to 76% at a temperature of 1150 °C – for the strain rate of $5 \cdot 10^{-3}\ s^{-1}$ and RA from 82% at a temperature of 1050 °C to 72% at a temperature of 1150°C – for the rate of $5 \cdot 10^{-3}\ s^{-1}$).

Hot ductility of examined steel in a temperature range from 1050 °C to 1150 °C fully correlates with the flow curves presented in Fig. 5 and Fig. 6. Dynamic recrystallization nucleuses in a highly stressed grain boundary area and fine dynamically recrystallized grains should isolate the micro-cracks from grain boundaries, thus improve ductility [32]. Moreover, Mintz and Abushosha [33] revealed that dynamic recrystallization and the movement of grain boundaries can counteract voids merging and consequently increase the values of RA. In a temperature range from 1150 °C to 1200 °C, the visablereduction in ductility was noted (Fig. 7). Moreover, surface topography of the sample after tension at the temperature of 1200 °C shows features of a mixed fracture. Intercrystalline fracture was revealed in some places (Fig. 10c), which is typical for alloys containing a significant fraction of brittle phases at grain boundaries or segregating atoms of admixtures – reducing the strength of grain boundaries. In this case, nucleation of micro-cracks usually takes place at the edges of grains, i.e. at the contact point of three grains during slip process along grain boundaries with weak influence of accommodative mechanisms, which are diffusion

creep and dislocation slip. Intercrystalline decohesion, characterized by the presence of flat grain surfaces (Fig. 10d), which is the result of the slip along grain boundaries, was also revealed on fracture surface of specimens subjected to tension at the temperature of 1200 °C. Similar effects was noted causes intercrystalline cracking. The above thesis is consistent with the works of Kang [25] and Hurtado-Delgado [34].Morphology and chemical composition in [32], where TWIP-type high-manganese steel, containing 22% Mn, was subjected to hot tension. One of the reason for significantly lower hot ductility of samples subjected to tension at the temperature of 1200 °C may be the presence of Nb(C,N) carbonitride precipitations at the austenite grain boundaries, which of non-metallic precipitations and inclusions, disclosed on longitudinal specimens near fracture area, are presented in Fig. 11-13.

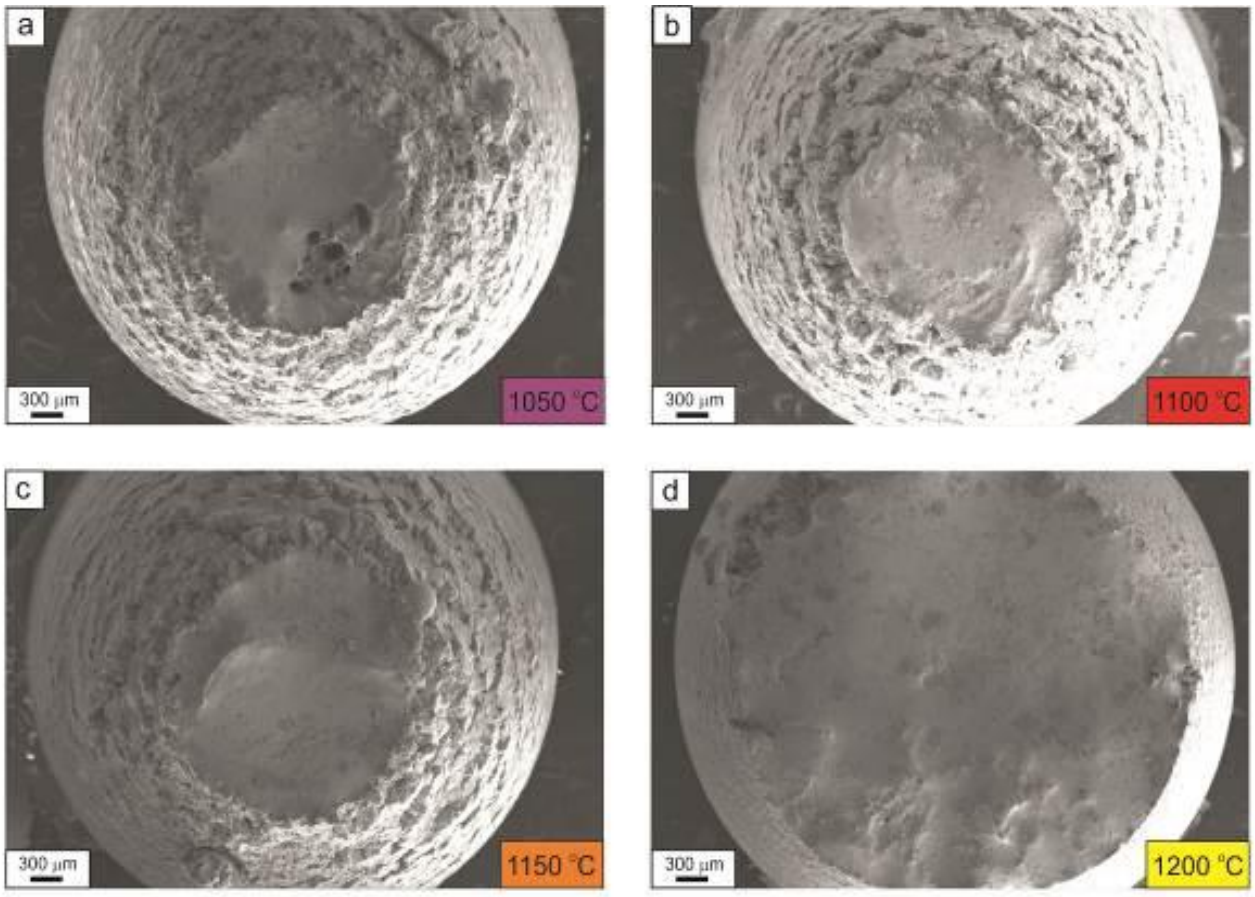

Fig. 9. Fractures of samples after tension at the temperature of: a) 1050 °C, b) 1100 °C, c) 1150 °C, d) 1200 °C (strain rate $5 \cdot 10^{-3}\ s^{-1}$)

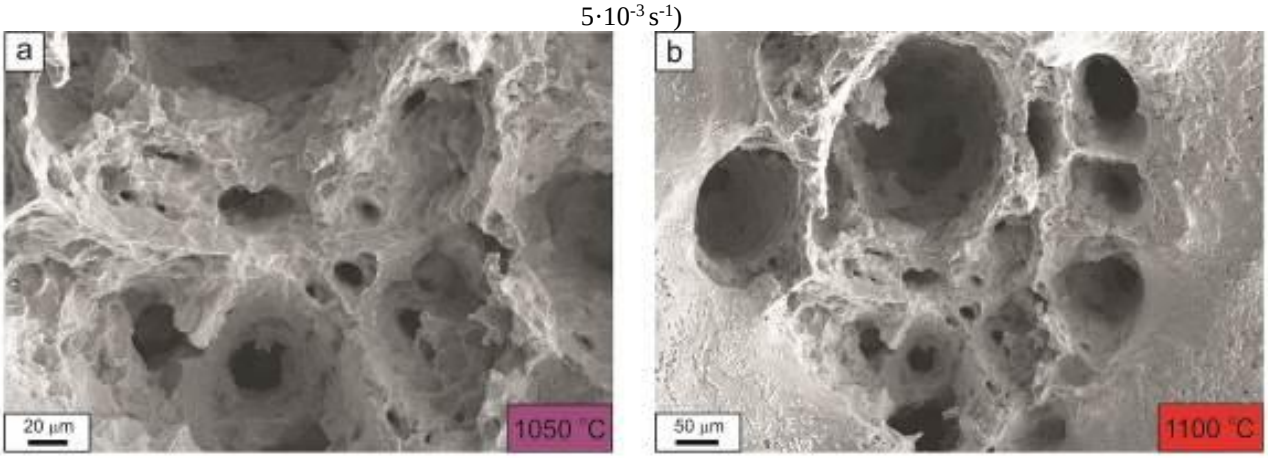

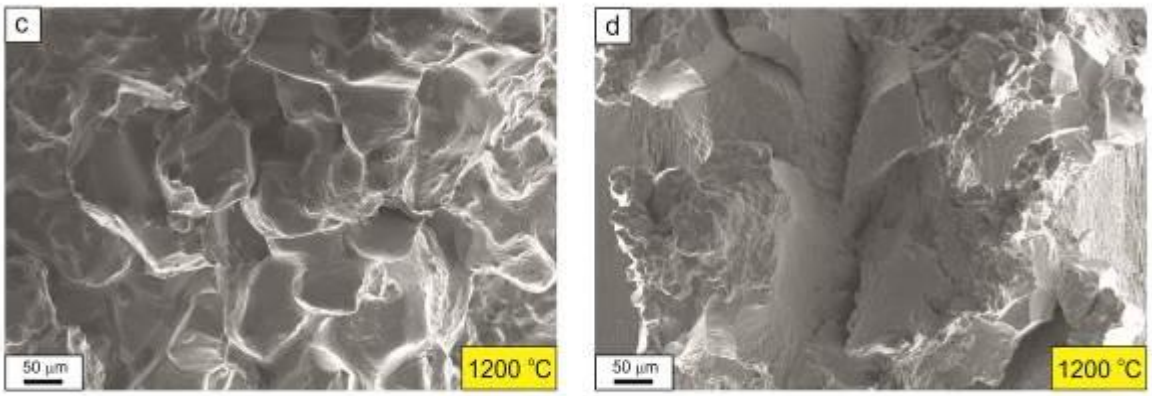

Fig. 10. Fractures of samples after hot tensile test: a, b) ductile fracture with numerous pits and voids of various size and depth, c) intercrystalline fracture; d) mixed fracture with visible cracks and flat grain surfaces (strain rate $5 \cdot 10^{-3}$ s^{-1})

Conducted analysis revealed the presence of single polygonal AlN nitrides (Fig. 12). In the large number of cases, complex MnS-AlN type particles with a MnS sulphide core were identified (Fig. 11 and Fig. 12). These results are consistent with those presented in the work of Liu et al. [31], where the influence of the presence of AlN particles on hot ductility of TWIP-type steel, containing 24% Mn and 1.4% Al, was investigated. It was shown in works [25, 35, 36] that the presence of AlN nitrides and MnS-AlN complex precipitations at the austenite grain boundaries may have unfavourable effect on the hot ductility and caused the intercrystalline embitterment. In the analyzed Fe-0.05C-24Mn-3.5Si-1.6Al austenitic steel – in fewer cases – the presence of globular MnS-type non-metallic inclusions, partially modified with rare earth elements was revealed (Fig. 13). Non-metallic inclusions of this form are difficult to deform in the process of plastic working and will not affect the anisotropy of plastic properties of products made of this steel.

Issues concerning the morphology of fracture surface after static hot tensile tests in high-manganese steels, as well as the impact of the presence of MnS-type non-metallic inclusions and complex MnS-AlN precipitations on cracking process of these steels were the subject of research in works [37-39]. Similarly as shown in [31], where the influence of Mn and Al content on hot ductility of Fe-xMn-C-yAl austenitic steels was investigated, MnS-type sulphides and MnS-AlN precipitations (also after modification with rare earth elements), may act as potential crack nucleation areas. It may be assumed that the initiation of cracks or micropores occurs on the revealed sulphides, and the stress may be transferred to these particles in the initial stage of plastic strain.

Microstructure of samples after tension, revealed on the longitudinal microsections near fracture area, is shown in Fig. 14. Heterogeneous microstructure of the sample subjected to tension at a temperature of 1050 °C, with marked zone of dynamically recrystallized grains, is shown in Fig. 15a. Average size of recrystallized austenite grains is equal to approximately 35 µm. Fig. 15b shows the microstructure of sample subjected to tension under the same conditions, revealed in the area away from the fracture front – without the presence of dynamically recrystallized grains. Microstructure of the specimen subjected to tension at the temperature of 1150 °C and rate of $5 \cdot 10^{-3}$ s^{-1} is shown in Fig. 15c. Grains, elongated in the direction of the applied stress, can be observed. On their boundaries, fine dynamically recrystallized necklace like grains were revealed. Figure 15d shows microstructure of the sample located near the fracture, after tensile test carried out at the temperature of 1200 °C.

The cracks visible in this figure, running along the boundaries of austenite grains or at the contact point of three grainsare the evidence of intercrystalline decohesion occurring as a result of slip along grain boundaries in the process of plastic strain. In the vicinity of fracture front, numerous micro-voids were also observed (marked with white ovals), which were probably formed in the initial stage of plastic deformation and were isolated by migration of grain boundaries [30]. Non-metallic inclusions, which were identified as AlN particles or MnS-AlN type complex precipitations, are also visible at the grain boundaries.

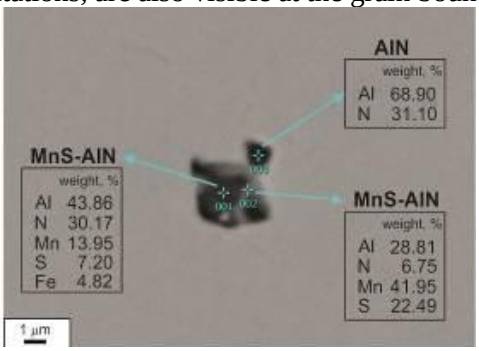

Fig. 11. Morphology and chemical composition of particles in Fe-0.05C-24Mn-3.5Si-1.6Al steel

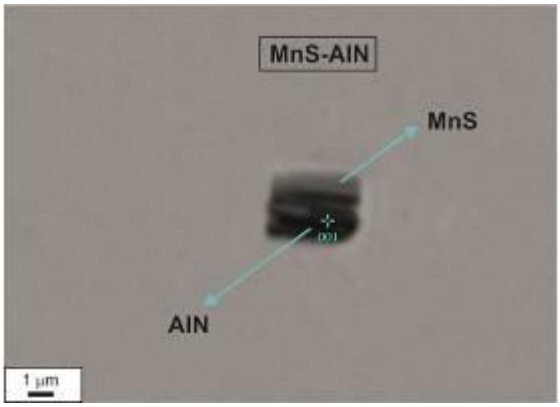

Fig. 12. View of the complex particle MnS-AlN-type in Fe-0.05C-24Mn-3.5Si-1.6Al steel

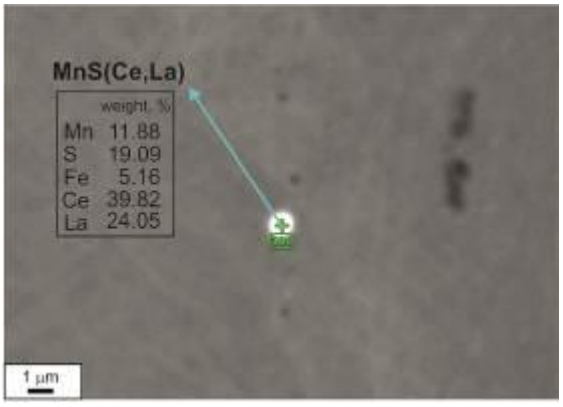

Fig. 13. The partially modified MnS-type inclusion in Fe-0.05C-24Mn-3.5Si-1.6Al steel

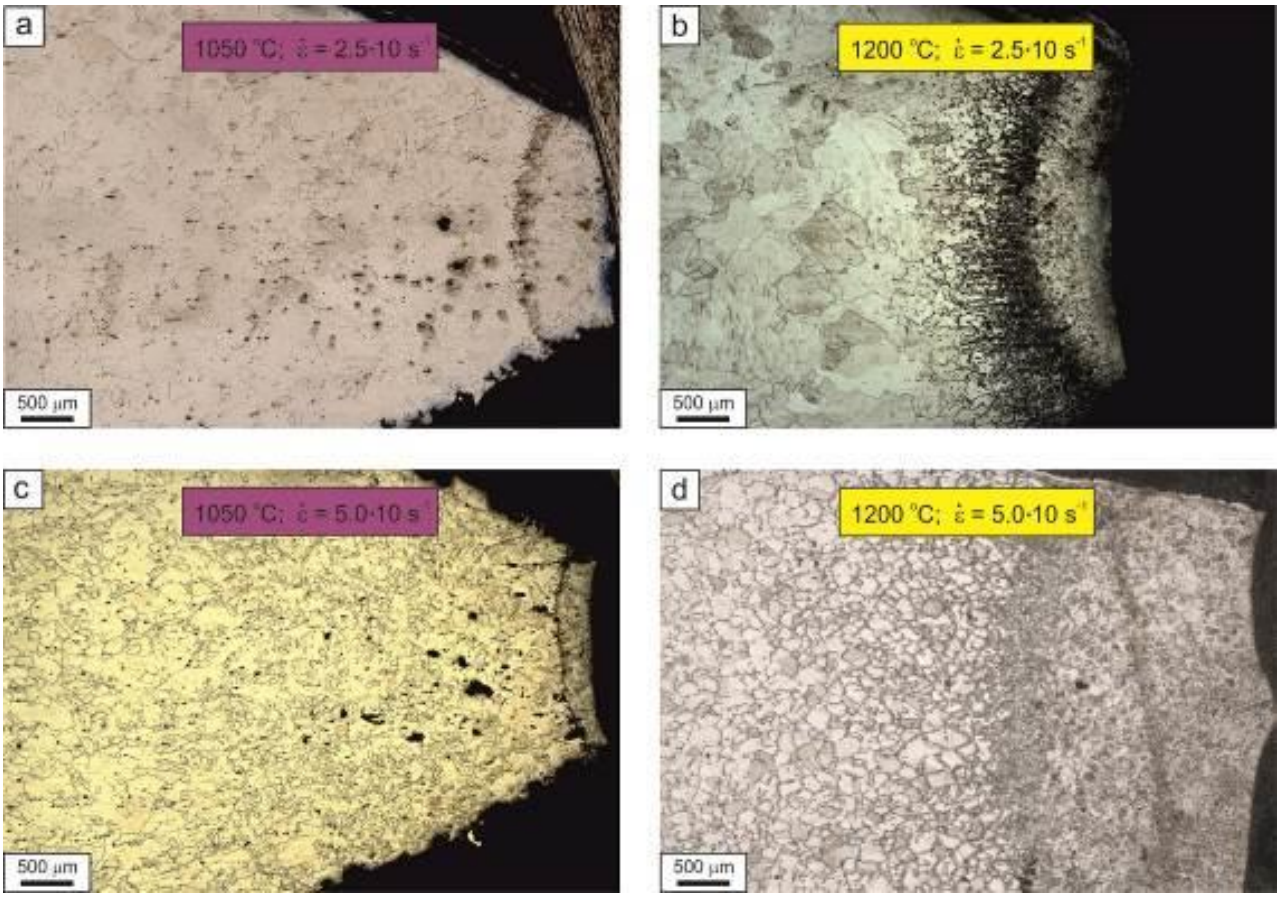

Fig. 14. Microstructures of samples after hot tensile test, revealed near the fracture area: a) and b) test temperature of 1050 °C and 1200 °C, strain rate of $2.5 \cdot 10^{-3}\ s^{-1}$ c) and d) test temperature of 1050 °C and 1200 °C; strain rate of $5 \cdot 10^{-3}\ s^{-1}$

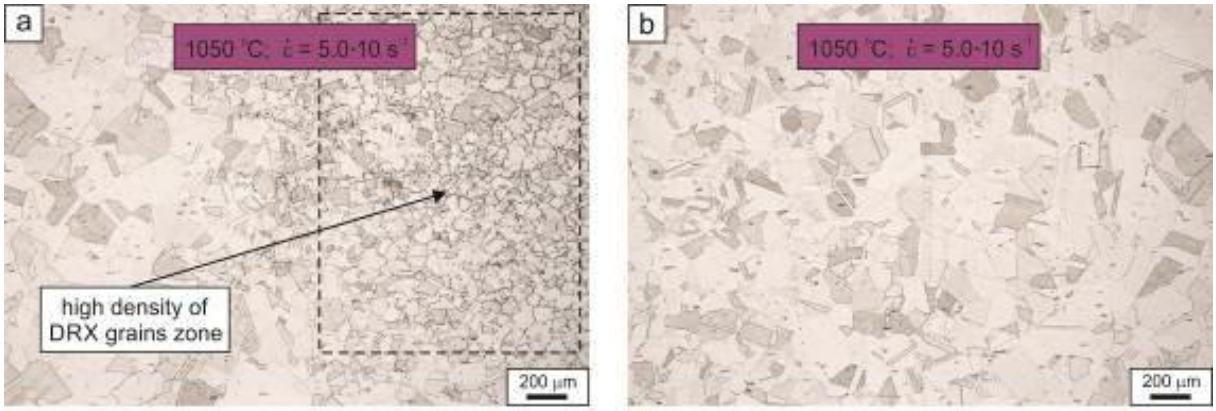

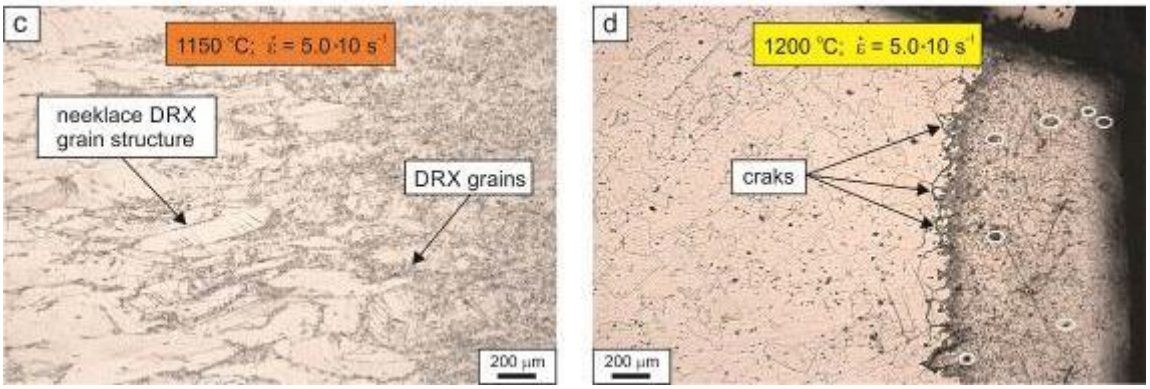

Fig. 15. Microstructure of samples after hot tensile test: a) and b) at the temperature of 1050 °C; c) at the temperature of 1150 °C; d) at the temperature of 1200 °C; (strain rate $5 \cdot 10^{-3}\ s^{-1}$)

4. CONCLUSIONS

Hot tensile tests performed on the Fe-0.05C-24Mn-3.5Si-1.6Al steel in a t emperature range from 1050 °C to 1200 °C revealed, that dynamic recrystallization is the main mechanism controlling the course of plastic deformation under mentioned conditions. An analysis of the stress-strain curves showed, as expected, that along with a decrease of testing temperature, the maximum values of the σ_m yield stress increase, while the ε_m strain shifts towards larger deformations. Higher values of maximum yield stresses in the examined temperature range were observed for the strain rate of $5 \cdot 10^{-3}\ s^{-1}$.

In a temperature range from 1050 °C to 1150 °C, studied steel is characterized by high ductility. The reduction in area in mentioned temperature range decreases from 90% to 76% – for the strain rate of $2.5 \cdot 10^{-3}\ s^{-1}$ and from 82% to 72% – for the strain rate of $5 \cdot 10^{-3}\ s^{-1}$.

Fractures of specimens, subjected to tension in a temperature range from 1050 °C to 1150 °C are ductile with the presence of numerous voids and pits of various size and depth. Fine dynamically recrystallized grains, produced in the process of plastic deformation, isolate micro-cracks from grain boundaries and thus improve ductility. Moreover, dynamic recrystallization and grain boundary movement counteract the aggregation of revealed voids and consequently increase the RA value. After exceeding the temperature of 1150 °C, there is a distinct decrease in ductility, regardless of the applied strain rate. Moreover,fractures of samples change into mixed with locally disclosed intercrystalline features, also with cracks and flat grain surfaces. The probable cause of the decreased ductility of examined steel at the temperature of 1200 °C should be the presence of AlN particles at grain boundaries and MnS-AlN type complex precipitations, which inhibit the process of dynamic recrystallization, favouring the slip along grain boundaries.

Acknowledgment

Publication supported as part of the Initiative of Excellence program - Research University at the Silesian University of Technology, 2022

5. REFERENCES

1. Sozańska-Jędrasik, L., Mazurkiewicz, J., Borek, W., Matus, K., (2018). *Carbides analysis of the high strength and low density Fe-Mn-Al-Si steels*. Archives of Metallury and Materials, 63(1), 265-276.

2. Śmiglewicz, A., Jabłońska, M., Płachta, A., Rodak, K., Michalik, R. (2016). *The effect of High Strain Rate on Properties and Microstructure of the fully Austenitic High Mn Steel*, Solid State Phenomena 246, 55-58.

3. Jabłońska, M., Śmiglewicz, A., Niewielski, G., (2015). *The effect of strain rate on the mechanical properties and microstructure of the high-Mn steel after dynamic deformation tests*, Archives of Metallurgy and Materials, 60, 123-126.

4. Yuan, X., Chen, L., Zhao, Y., Di, H., Zhu, F., (2015). *Influence of annealing temperature on mechanical properties and microstructures of a high manganese austenitic steel*, Journal of Materials Processing Technology, 217, 278-285

5. Shen, Y.S., Qiu, C.H., Wang, L., Sun, X., Zhao, X.M., Zuo, L., (2013). *Effects of cold rolling on microstructure and mechanical properties of Fe-30Mn-3Si-4Al-0.093C TWIP steel*, Materials Science and Engineering A, 561, 329-337.

6. Wang, X., Sun, X., Song, C., Chen, H., Tong, S., Han, W., Pan, F. (2018). *Evolution of microstructures and mechanical properties during solution treatment of a Ti–V–Mo-containing high-manganese cryogenic steel*, Materials Characterization, 135, 287–294.

7. Park, K.T., Hwang, S.W, Ji, J.H., Lee, C.S. (2011). *Static and dynamic deformation of fully austenitic high Mn steels*, Procedia Engineering, 10, 1002-1006.

8. Pierce, D.T., Jiménez, J.A., Bentley, J. Raabe, D., Wittig, J.E., (2015). *The influence of stacking fault energy on the microstructural and strain hardening*

evolution of Fe–Mn–Al–Si steels during tensile deformation, Acta Materialia, 100, 178-190.
9. Peng, X., Zhu, D., Hu, Z., Yi, W., Liu, H., Wang, M., (2013). *Stacking fault energy and tensile deformation behavior of high-carbon twinning-induced plasticity steels: Effect of Cu addition*, Materials & Design, 45, 518-523.
10. De Cooman, B.C., Estrin, Y.; Kim, S.K., (2018). *Twinning-induced plasticity (TWIP) steels*. Acta Materialia, 142, 283-362.
11. Jabłońska, M., (2014). *Mechanical properties and fractographic analysis of high manganese steels after dynamic deformation tests*, Archives of Metallurgy and Materials , 59, 1193-1197.
12. Wu, Z.Q., Tang, Z.Y., Li, H.Y., Zhang, H.D. (2012). *Effect of strain rate on microstructure evolution and mechanical behavior of a low C high Mn TRIP/TWIP steels*, Acta Metallurgica Sinica, 48, 593-600.
13. Frommeyer, G., Brux, U., Neumann, P. (2003). *Supra-ductile and high-strength manganese TRIP/TWIP steels for high energy absorption purposes*, Iron and Steel Institute of Japan International, 43, 438-446.
14. Opiela, M., Fojt-Dymara, G., Grajcar A., Borek, W., (2020). *Effect of grain size on the microstructure and strain hardening behavior of solution heat-treated low-C high-Mn steel*, Materials, 13, 1-13.
15. Allain, S., Chateau, J.-P., Bouaziz, O., (2004). *A physical model of the twinning-induced plasticity effect in a high manganese austenitic steel*, Materials Science and Engineering A, 387, 143-147.
16. Kim, J.K., Chen, L., Kim, H.S., Kim, S.K., Estrin, Y., Cooman, B. (2009). *On the Tensile Behavior of High-Manganese Twinning-Induced Plasticity Steel*, Metallurgical and Materials Transactions A, 40, 3147-3158.
17. Ueji, R., Tsuchida, N., Terada, D., Tsuji, N., Tanaka, Y., Takemura, A. et al., (2008). *Tensile properties and twinning behavior of high manganese austenitic steel with fine-grained structure*, Scripta Materialia, 59(9), 963-966.
18. Dobrzański, L.A., Borek, W., Mazurkiewicz, J., (2016). *Effect of strain deformation rates on forming the structure and mechanical properties of high-manganese austenitic TWIP steels*, Advanced Materials and Process Technology, 2(4), 490-502.
19. Yang, C., Zhang, Z., Zhang, P., Zhang, Z., (2017). *The premature necking of twinning-induced plasticity steels*, Acta Materialia, 136, 1-10.
20. Mintz, B., Qaban, A., (2021). *Understanding the high temperature side of the hot ductility curve for steels*, Materials Science and Technology, 37, 237-249.
21. Mintz, B., Yue, S., Jonas, J.J., (1991). *Hot ductility of steels and its relationship to the problem of transverse cracking during continuous casting*, International Materials Reviews, 36, 187-217.
22. Mintz, B., (1999). *The influence of composition on the hot ductility of steels and to the problem of transverse cracking*, ISIJ International, 39, 833-255.
23. Kang, S.E., Banerjee. J.R., Mintz. B. (2012) *Influence of S and AlN on hot ductility of high Al, TWIP steels*, Materials Science and Technology, 28, 589-596.
24. Kang, S.E., Banerjee, J.R., Tuling, A.S., (2014). *The influence of B on the hot ductility of high Al, and high Al-Nb, TWIP steels*, Materials Science and Technology, 30, 486-494.
25. Kang, S.E., Kang, M.H., Mintz, B. (2021). *Influence of vanadium, boron and titanium on hot ductility of high Al, TWIP steels*, Materials Science and Technology, 37, 42-58.
26. Kang, S.E., Tuling, A., Lau, I. (2011). *The hot ductility of NbV containing high Al, TWIP steels*, Materials Science and Technology, 27, 909-915.
27. Wang, Y., Zhao S., Song, R., Hu, B., (2021). *Hot ductility behawior of a Fe-0.3C-9Mn-2Al medium Mn steel*, International Journal of Minerals, Metallurgy and Materials, 28(6355), 1-8.
28. Qaban, A., Mintz, B., Kang, S.E., Naher, S., (2017). *Hot ductility of high Al TWIP steels containing Nb and Nb-V*, Materials Science and Technology; doi.org/10.1080/02670836.2017.130907
29. Mejia, I., Salas-Reyes, A.E., Calvo, J., Cabrera, J.M., (2015). *Effect of Ti and B microadditions on the hot ductility behavior of a high-Mn austenitic Fe-23Mn-1.5Al-1.3Si-0.5C TWIP steel*, Materials Science & Engineering A, 648, 311-329.
30. Lan, P., Tang, H., Zhang, J., (2016). *Hot ductility of high alloy Fe-Mn-C austenite TWIP steel*, Materials Science & Engineering A, 660, 127-138.
31. Liu, H., Liu, J., Wu, B., Shen, Y., He, Y., Ding, H., Su, H., (2017). *Effect of Mn and Al contents on hot ductility of high alloy Fe-xMn-C-yAl austenite TWIP steels*, Materials Science & Engineering A, 708, 360-374.
32. Hamada, A.S., Karlajainen, I.P., (2011). *Hot ductility behaviour of high-Mn TWIP steels*, Materials Science & Engineering A, 528, 1819-1827.
33. Mintz, B., Abushosha, R., (1992). *Effectiveness of hot tensile test in simulating strainghtening in continuous casting*, Materials Science and Technology, 8, 171-178.
34. Hurtado-Delgado, E., Morales, R.D., (2001). *Hot ductility and fracture mechanisms of a C-Mn-Nb-Al steel*, Metallurgical and Materials Transactions B, 32, 919-927.
35. Liu, H., Liu, J., Michelic, S.K., Wei, F.W, Zhuang, C., Li, S.Q., (2016). *Characteristic of AlN particles in low carbon Fe-Mn-Si-Al TWIP steel produced by AOD-ESR method*, Ironmaking & Steelmaking, 43, 171-179.

36. Liu, H., Liu, J., Michelic, S.K., Shen, S.B, Su, X.F., Wu, B.W., Dinh, H. (2016). *Characterization and analysis of non-metallic inclusions in low carbon Fe-Mn-Si-Al TWIP steels*, Steel Research International, 87, 1723-1732.
37. Madivala, M., Schwedt, A., Prahl, U., Bleck, W., (2019). *Strain hardening, damage and fracture behavior of Al-added high Mn TWIP steels*, Metals, 9(3), 367, doi.org/10.3390/met9030367.
38. Kyutae, H., Jaehong, Y., Bongkeun, L., Ilwook, H., Changhee, L., (2014). *Effect of Ni on the hot ductility and hot cracking susceptibility of high Mn austenitic cast steel*, Materials Science & Engineering A, 2, 618, 295-304.
39. Yang, C.L., Zhang, Z.J., Zhang, P., Zhang, Z.F., (2017). *The premature necking of twining-induced plasticity steels*, Acta Materialia, 136, 1-10.

Received: May 18, 2022 / Accepted: December 15, 2022 / Paper available online: December 20, 2022